LBL-25769
UC-403

Lawrence Berkeley Laboratory
UNIVERSITY OF CALIFORNIA

EARTH SCIENCES DIVISION

The Effect of Precipitation on Contaminant Dissolution and Transport: Analytic Solutions

W.B. Light, P.L. Chambré, T.H. Pigford, and W.W.-L. Lee

September 1988

HYDROLOGY DOCUMENT NUMBER 469

Prepared for the U.S. Department of Energy under Contract Number DE-AC03-76SF00098.

DISCLAIMER

This document was prepared as an account of work sponsored by the United States Government. Neither the United States Government nor any agency thereof, nor The Regents of the University of California, nor any of their employees, makes any warranty, express or implied, or assumes any legal liability or responsibility for the accuracy, completeness, or usefulness of any information, apparatus, product, or process disclosed, or represents that its use would not infringe privately owned rights. Reference herein to any specific commercial products process, or service by its trade name, trademark, manufacturer, or otherwise, does not necessarily constitute or imply its endorsement, recommendation, or favoring by the United States Government or any agency thereof, or The Regents of the University of California. The views and opinions of authors expressed herein do not necessarily state or reflect those of the United States Government or any agency thereof or The Regents of the University of California and shall not be used for advertising or product endorsement purposes.

Printed in the United States of America
Available from
National Technical Information Service
U.S. Department of Commerce
5285 Port Royal Road
Springfield, VA 22161
Price Code: A02

Lawrence Berkeley Laboratory is an equal opportunity employer.

UCB-NE-4127
LBL-25769

The Effect of Precipitation on Contaminant Dissolution and Transport: Analytic Solutions

W. B. Light, P. L. Chambré, T. H. Pigford, and W. W.-L. Lee

Department of Nuclear Engineering
University of California

and

Earth Sciences Division
Lawrence Berkeley Laboratory
1 Cyclotron Road
Berkeley, California 94720

September 1988

This work was supported in part by the Manager, Chicago Operations, Repository Technology and Transportation Program, of the U.S. Department of Energy under Contract No. DE-AC03-76SF00098.

The authors invite comments and would appreciate being notified of any errors in the report.

T. H. Pigford
Department of Nuclear Engineering
University of California
Berkeley, CA 94720

Contents

1. Introduction 1

2. Background 1

3. Analysis 2

4. Numerical Illustrations 10

5. Conclusions 11

References 12

List of Figures

Figure 1. The stationary precipitation front.

Figure 2. Schematic of concentration profiles.

Figure 3. Dimensionless mass-transfer rate out from waste surface (upper curves) and precipitation front (lower curves) for $\alpha = 5000$, $C_o/C_p = 1000$.

Figure 4. Dimensionless mass-transfer rate out from waste surface (upper curves) and precipitation front (lower curves) for $\alpha = 500$, $C_o/C_p = 1000$.

Figure 5. Dimensionless mass-transfer rate out from waste surface (upper curves) and precipitation front (lower curves) for $\alpha = 50$, $C_o/C_p = 1000$.

1. Introduction

Waste material in a geologic repository will eventually dissolve and migrate away. For many waste components, this process will be limited by the solubility of the waste matrix and species involved. In this paper we deal with a single contaminant species and analyze the effect of precipitation caused by a reduced solubility of the contaminant at some distance from the waste package. The precipitation may be due to local geochemical changes such as changes in temperature, *p*H or redox potential, caused by nearby geologic features or the waste itself.

If precipitation occurs it will be necessary to identify the key parameters in the precipitation process so that they can be studied in laboratory and field experiments. In addition to identifying the parameters that affect dissolution rate, this study shows how the precipitation process can be incorporated in the performance assessments of nuclear waste disposal.

If the U. S. Nuclear Regulatory Commission's release rate requirement[1] for the engineered barrier system is to be met at the waste package/rock interface, precipitation can increase the mass transport rate near the waste package, and must be considered in showing compliance with the release rate criterion.

In contrast with other works on precipitation fronts,[2,3,4,5,6] we provide analytic solutions to the problem of precipitation at a stationary front. Numerical illustrations of these solutions are also presented.

2. Background

Garisto and Garisto[2,4] and Garisto[3] have studied the effect of a stationary precipitation front near the waste on the dissolution rate of a spent fuel waste package. They predict enhanced dissolution rates affecting not only the matrix but any congruently released contaminant as well. However, they did not state the *raison dêtre* for a stationary precipitation front.

One way that a stationary precipitation front can exist is by alpha radiolysis. Radioactive waste in contact with water may produce an excess of oxidation products by alpha radiolysis. If hydrogen gas escapes, the remaining radiolysis products, oxygen and hydrogen peroxide, can create a local oxidizing environment near the waste. This would create a region of high redox potential around the waste where most actinide compounds show higher solubility than in the surrounding region of lower redox potential.

Neretnieks[7] has postulated a redox front where hydrogen peroxide oxidizes ferrous iron from granitic rock

near the high-level nuclear waste. He estimates a front velocity of about 0.06 mm/yr. In a separate paper Neretnieks[8] has considered the effect of such a moving redox front on uranium transport away from the oxidized region. He was not concerned with the effect on the rate of dissolution of the waste itself. Because a nearby precipitation front can increase the net rate of dissolution of the solubility-limited waste matrix, such as uranium in spent fuel, it can also increase the release rate of species that are released congruently with matrix dissolution.

This report presents an analytic solution to predict contaminant dissolution rates, as well as mass-transfer rates into the far field, based on transport by diffusion through a porous medium with spatially dependent contaminant solubility.

The analysis is formulated for a step-function reduction in the solubility from C_e to C_p at position r_p, but it is applicable to any system in which the solubility of a contaminant decreases with distance from the contaminant source and is constant with time.

The contaminant will dissolve from the waste surface and travel outward down the concentration gradient. At early times, concentrations are quite low so that a solubility limit is not met in the porous rock away from the waste surface. Eventually, as the concentration increases, the solution may become locally saturated and precipitation will begin. The concentration will continue to rise in the region between the waste package surface and the precipitation front, finally reaching a steady-state profile.

Where there is local saturation, precipitate will form at a rate so as to balance the net rates of mass transfer into and out of the saturated region. For a sharp precipitation front, as postulated here, the saturated region is reduced to a surface with zero thickness. In reality, the front could extend over a non-zero transition thickness.[9] We also neglect the effect the accumulating precipitate might have on the transport process, such as filling the pores or moving as a colloid. The results presented here accurately describe the case of a sharp front and also provide a qualitative picture of systems wherein the solubility profile is a smooth function of distance.

3. Analysis

As illustrated in Figure 1, a spherical waste solid of radius r_e is embedded in an infinite water-saturated porous medium. There is no contaminant in the porous medium when dissolution begins at time $t = 0$, and direct contact is assumed between the waste and the porous medium (no container or other barriers). The solubility discontinuity, or precipitation front, is assumed to be a concentric spherical shell of radius

r_p surrounding the waste package (Figure 1). The dissolution rate at the waste surface is assumed to be governed by a linear solid-liquid reaction-rate expression with the forward reaction rate j_o occurring when there is no contaminant in the pore water and the minimum rate, zero, approached as the contaminant concentration in the pore water approaches the solubility limit at the waste surface (see Equation (4)). In the limit when j_o becomes sufficiently large, the concentration at the waste surface quickly reaches the surface solubility C_o and the expression reduces to that for a constant concentration boundary condition, C_o.

Transport in the porous medium is by fluid-phase diffusion only, with no advection. Local sorption equilibrium is assumed, and radioactive decay is neglected.

The precipitation front is assumed to be at a known, fixed location, r_p. At early times, when the concentration is below the solubility limit at the front location, the front has no effect on the transport process. The domain from the waste surface to infinity is then treated as a single homogeneous region and we have

$$\frac{\partial C_1}{\partial t} = \frac{D}{K}\frac{1}{r^2}\frac{\partial}{\partial r}\left(r^2\frac{\partial C_1}{\partial r}\right), \qquad r_o < r < \infty, \quad 0 < t < t_p \tag{1}$$

where $C_1(r,t)$ is the fluid-phase contaminant concentration for $r_o < r < \infty$ and $0 < t < t_p$, D is the contaminant diffusion coefficient in the pore fluid, K is the retardation coefficient, and t_p is the time at which the solubility limit is reached and precipitation begins. The initial concentration and the concentration at infinity are both assumed to be zero

$$C_1(r,0) = 0, \qquad r_o < r < \infty \tag{2}$$

$$\lim_{r\to\infty} C_1(r,t) = 0, \qquad 0 < t < t_p \tag{3}$$

The dissolution rate at the waste surface is set equal to the assumed concentration-dependent reaction-rate law

$$-\epsilon D\frac{\partial C_1}{\partial r}\bigg|_{r=r_o} = j_o\left(1-\frac{C_1}{C_o}\right)\bigg|_{r=r_o}, \qquad 0 < t < t_p \tag{4}$$

where ϵ is the porosity and j_o is the forward dissolution reaction rate per unit surface area of waste. To determine the precipitation time, t_p, we first solve (1)-(4). The contaminant concentration predicted by (1)-(4) increases steadily with time and monotonically decreases with distance from the waste (Figure 2, $t < t_p$). Although it is possible that the concentration may never reach the solubility limit anywhere other than the waste surface, if precipitation does occur we can determine t_p implicitly from the equation

$$C_1(r_p, t_p) = C_p \tag{5}$$

For $t > t_p$ we divide the domain into two regions, one inside the front and the other outside the front. For the inner region

$$\frac{\partial C_2}{\partial t} = \frac{D}{K}\frac{1}{r^2}\frac{\partial}{\partial r}\left(r^2\frac{\partial C_2}{\partial r}\right), \qquad r_o < r < r_p, \quad t_p < t < \infty \tag{6}$$

where $C_2(r,t)$ is the contaminant concentration for $r_o < r < r_p$ and $t_p < t < \infty$. The initial condition for this problem is given by the solution to (1)-(4) at $t = t_p$

$$C_2(r,t_p) = C_1(r,t_p), \qquad r_o < r < r_p \tag{7}$$

The boundary condition at the waste surface is the reaction-rate law as before, with C_2 replacing C_1

$$-\epsilon D\frac{\partial C_2}{\partial r}\bigg|_{r=r_o} = j_o\left(1-\frac{C_2}{C_o}\right)\bigg|_{r=r_o}, \qquad t_p < t < \infty \tag{8}$$

At the new boundary, $r = r_p$, we set the concentration to the solubility limit C_p

$$C_2(r_p,t) = C_p, \qquad t_p < t < \infty \tag{9}$$

The region outside the precipitation front is treated similarly

$$\frac{\partial C_3}{\partial t} = \frac{D}{K}\frac{1}{r^2}\frac{\partial}{\partial r}\left(r^2\frac{\partial C_3}{\partial r}\right), \qquad r_p < r < \infty, \quad t_p < t < \infty \tag{10}$$

with side conditions

$$C_3(r,t_p) = C_1(r,t_p), \qquad r_p < r < \infty \tag{11}$$

$$C_3(r_p,t) = C_p, \qquad t_p < t < \infty \tag{12}$$

$$\lim_{r\to\infty} C_3(r,t) = 0, \qquad t_p < t < \infty \tag{13}$$

To solve the equation system (1)-(13) we first introduce the following dimensionless parameters

$$\rho \doteq r/r_o, \qquad \rho_p \doteq r_p/r_o$$

$$\tau \doteq tD/Kr_o^2, \qquad \tau_p \doteq t_pD/Kr_o^2$$

$$\alpha \doteq \frac{j_o r_o}{\epsilon D C_o}, \qquad \alpha' \doteq \alpha + 1$$

The problem is then simplified by introducing new dependent variables

$$u_1(\rho,\tau) \doteq \rho C_1(\rho,\tau)/C_o, \qquad u_2(\rho,\tau) \doteq \rho C_2(\rho,\tau)/C_o, \qquad u_3(\rho,\tau) \doteq \rho C_3(\rho,\tau)/C_o$$

The reformulated equations appear as the following system of equations (14)-(26)

$$\frac{\partial u_1(\rho,\tau)}{\partial \tau} = \frac{\partial^2 u_1(\rho,\tau)}{\partial \rho^2}, \qquad 1 < \rho < \infty, \quad 0 < \tau < \tau_p \tag{14}$$

$$u_1(\rho,0) = 0, \qquad 1 < \rho < \infty \tag{15}$$

$$-\left.\frac{\partial u_1(\rho,\tau)}{\partial \rho}\right|_{\rho=1} = \alpha - \alpha' u_1(1,\tau), \qquad 0 < \tau < \tau_p \tag{16}$$

$$\lim_{\rho\to\infty} \frac{u_1(\rho,\tau)}{\rho} = 0, \qquad 0 < \tau < \tau_p \tag{17}$$

$$u_1(\rho_p,\tau_p) = \rho_p C_p / C_o \tag{18}$$

$$\frac{\partial u_2(\rho,\tau)}{\partial \tau} = \frac{\partial^2 u_2(\rho,\tau)}{\partial \rho^2}, \qquad 1 < \rho < \rho_p, \quad \tau_p < \tau < \infty \tag{19}$$

$$u_2(\rho,\tau_p) = u_1(\rho,\tau_p), \qquad 1 < \rho < \rho_p \tag{20}$$

$$-\left.\frac{\partial u_2(\rho,\tau)}{\partial \rho}\right|_{\rho=1} = \alpha - \alpha' u_2(1,\tau), \qquad \tau_p < \tau < \infty \tag{21}$$

$$u_2(\rho_p,\tau) = \rho_p C_p / C_o, \qquad \tau_p < \tau < \infty \tag{22}$$

$$\frac{\partial u_3(\rho,\tau)}{\partial \tau} = \frac{\partial^2 u_3(\rho,\tau)}{\partial \rho^2}, \qquad \rho_p < \rho < \infty, \quad \tau_p < \tau < \infty \tag{23}$$

$$u_3(\rho,\tau_p) = u_1(\rho,\tau_p), \qquad \rho_p < \rho < \infty \tag{24}$$

$$u_3(\rho_p,\tau) = \rho_p C_p / C_o, \qquad \tau_p < \tau < \infty \tag{25}$$

$$\lim_{\rho\to\infty} \frac{u_3(\rho,\tau)}{\rho} = 0, \qquad \tau_p < \tau < \infty \tag{26}$$

To solve (14)-(17), the Laplace transform of (14) is taken with respect to τ using the initial condition (15) with the result

$$sU_1(\rho,s) = \frac{\partial^2 U_1(\rho,s)}{\partial \rho^2}, \qquad 1 < \rho < \infty \tag{27}$$

where $U_1(\rho,s)$ is the Laplace transform of $u_1(\rho,\tau)$. The general solution to (27) taking into account boundary condition (17) is

$$U_1(\rho,s) = G(s)e^{-\rho\sqrt{s}} \tag{28}$$

where $G(s)$ is an arbitrary function. The transform of boundary condition (16) is

$$-\left.\frac{\partial U_1(\rho,s)}{\partial\rho}\right|_{\rho=1} = \frac{\alpha}{s} - \alpha' U_1(1,s) \tag{29}$$

Substituting (28) into (29) determines $G(s)$ and we get

$$U_1(\rho,s) = \frac{\alpha}{s(\alpha'+\sqrt{s})}\exp\left(-(\rho-1)\sqrt{s}\right), \qquad 1<\rho<\infty \tag{30}$$

The inverse transform is given by Abramowitz and Stegun (29.3.89)[10]

$$u_1(\rho,\tau) = \frac{\alpha}{\alpha'}\left[\operatorname{erfc}\left(\frac{\rho-1}{2\sqrt{\tau}}\right) - \exp\left(\alpha'(\rho-1)+\alpha'^2\tau\right)\operatorname{erfc}\left(\alpha'\sqrt{\tau}+\frac{\rho-1}{2\sqrt{\tau}}\right)\right], \qquad \begin{matrix}1<\rho<\infty\\ 0<\tau<\tau_p\end{matrix} \tag{31}$$

The final solution to (1)-(4) is then

$$C_1(\rho,\tau) = \frac{C_o}{\rho}\frac{\alpha}{\alpha'}\left[\operatorname{erfc}\left(\frac{\rho-1}{2\sqrt{\tau}}\right) - \exp\left(\alpha'(\rho-1)+\alpha'^2\tau\right)\operatorname{erfc}\left(\alpha'\sqrt{\tau}+\frac{\rho-1}{2\sqrt{\tau}}\right)\right], \qquad \begin{matrix}1<\rho<\infty\\ 0<\tau<\tau_p\end{matrix} \tag{32}$$

For the parameter values likely in a wet-rock repository[2], α is much greater than unity so that α/α' is approximately equal to unity. Two of the three ratios ρ_p, τ_p, and C_p/C_o must be specified with the third determined by (18). We have chosen to specify the front location and the solubility ratio and to determine the precipitation time τ_p numerically using (18) and (31).

To solve (19)-(22), we assume a solution form $u_2(\rho,\tau) = v_2(\rho) + w_2(\rho,\tau)$ where $v_2(\rho)$ is the steady-state solution and $w_2(\rho,\tau)$ is the transient component of the given problem. The steady-state equations for $v_2(\rho)$ are those given by (19), (21) and (22) with the time derivative set equal to zero

$$v_2''(\rho) = 0, \qquad 1<\rho<\rho_p \tag{33}$$

$$-v_2'(1) = \alpha - \alpha' v_2(1) \tag{34}$$

$$v_2(\rho_p) = \rho_p C_p/C_o \tag{35}$$

The solution to (33)-(35) is

$$v_2(\rho) = a\rho + b, \qquad 1<\rho<\rho_p \tag{36}$$

with

$$a = \frac{\rho_p(\alpha'/\alpha)(C_p/C_o) - 1}{\rho_p(\alpha'/\alpha) - 1}$$

$$b = \frac{\rho_p(1 - C_p/C_o)}{\rho_p(\alpha'/\alpha) - 1}$$

We now solve the following problem for $w_2(\rho,\tau)$ so that the combined solution $v_2(\rho) + w_2(\rho,\tau)$ satisfies the governing equations (19)-(22)

$$\frac{\partial w_2(\rho,\tau)}{\partial \tau} = \frac{\partial^2 w_2(\rho,\tau)}{\partial \rho^2}, \qquad 1 < \rho < \rho_p, \quad \tau_p < \tau < \infty \tag{37}$$

$$w_2(\rho,\tau_p) = u_1(\rho,\tau_p) - v_2(\rho), \qquad 1 < \rho < \rho_p \tag{38}$$

$$-\left.\frac{\partial w_2(\rho,\tau)}{\partial \rho}\right|_{\rho=1} = -\alpha' w_2(1,\tau), \qquad \tau_p < \tau < \infty \tag{39}$$

$$w_2(\rho_p,\tau) = 0, \qquad \tau_p < \tau < \infty \tag{40}$$

To solve (37)-(40), let $w_2(\rho,\tau) = \phi(\rho)\psi(\tau)$, then by (37)

$$\psi'(\tau) = -\lambda\psi(\tau) \tag{41}$$

and

$$\phi''(\rho) = -\lambda\phi(\rho) \tag{42}$$

The boundary conditions (39) and (40) are applied to the new solution form to get

$$-\phi'(1) = -\alpha'\phi(1) \tag{43}$$

$$\phi(\rho_p) = 0 \tag{44}$$

Equations (42)-(44) are solved to yield the eigenfunctions

$$\phi_n(\rho) = \sin\left[\sqrt{\lambda_n}(\rho_p - \rho)\right], \qquad 1 < \rho < \rho_p \tag{45}$$

with the eigenvalues λ_n determined by the solution to

$$\tan\left[\sqrt{\lambda_n}(\rho_p - 1)\right] = -\frac{\sqrt{\lambda_n}}{\alpha'} \tag{46}$$

The eigenvalues are determined numerically by intersecting the curves $y = \tan x$ and $y = -x/\alpha'(\rho_p - 1)$ with one eigenvalue $\lambda_n = (x_n/(\rho_p - 1))^2$ for each intersection point (x_n, y_n), $x_n > 0$. The corresponding $\psi_n(\tau)$ function from (41) is chosen to be

$$\psi_n(\tau) = e^{-\lambda_n(\tau - \tau_p)}, \qquad \tau_p < \tau < \infty \tag{47}$$

To meet the initial condition (39), the $\phi_n(\rho)\psi_n(\tau)$ solutions are superposed to get the infinite series solution

$$w_2(\rho, \tau) = \sum_{n=1}^{\infty} A_n \phi_n(\rho)\psi_n(\tau), \qquad 1 < \rho < \rho_p, \quad \tau_p < \tau < \infty \tag{48}$$

where the series coefficients are given by

$$A_n = \frac{1}{||\phi_n||^2} \int_1^{\rho_p} \phi_n(\rho)\left[u_1(\rho, \tau_p) - v_2(\rho)\right] d\rho$$

with the eigenfunction norm defined as

$$||\phi_n||^2 \doteq \int_1^{\rho_p} \phi_n^2(\rho) d\rho$$

The final solution to (6)-(9) is then

$$C_2(\rho, \tau) = C_o \left[a + \frac{b}{\rho} + \frac{1}{\rho} \sum_{n=1}^{\infty} A_n \phi_n(\rho)\psi_n(\tau)\right], \qquad 1 < \rho < \rho_p, \quad \tau_p < \tau < \infty \tag{49}$$

To solve (23)-(26), we assume again the solution form $u_3(\rho, \tau) = v_3(\rho) + w_3(\rho, \tau)$ where $v_3(\rho)$, the steady-state solution, is to satisfy

$$v_3''(\rho) = 0, \qquad \rho_p < \rho < \infty \tag{50}$$

$$v_3(\rho_p) = \rho_p C_p / C_o \tag{51}$$

$$\lim_{\rho \to \infty} \frac{v_3(\rho)}{\rho} = 0 \tag{52}$$

and $w_3(\rho, \tau)$, the transient component, is to satisfy

$$\frac{\partial w_3(\rho, \tau)}{\partial \tau} = \frac{\partial^2 w_3(\rho, \tau)}{\partial \rho^2}, \qquad \rho_p < \rho < \infty, \quad \tau_p < \tau < \infty \tag{53}$$

$$w_3(\rho, \tau_p) = u_1(\rho, \tau_p) - v_3(\rho), \qquad \rho_p < \rho < \infty \tag{54}$$

$$w_3(\rho_p, \tau) = 0, \qquad \tau_p < \tau < \infty \tag{55}$$

$$\lim_{\rho \to \infty} \frac{w_3(\rho, \tau)}{\rho} = 0, \qquad \tau_p < \tau < \infty \tag{56}$$

The solution to (50)-(52) is

$$v_3(\rho) = \rho_p C_p / C_o, \qquad \rho_p < \rho < \infty \tag{57}$$

To solve (53)-(56) we first shift the space-time boundaries by letting $x = \rho - \rho_p$ and $y = \tau - \tau_p$ to get the resulting new equations

$$\frac{\partial w_3(x,y)}{\partial y} = \frac{\partial^2 w_3(x,y)}{\partial x^2}, \qquad 0 < x < \infty, \quad 0 < y < \infty \tag{58}$$

$$w_3(x,0) = u_1(x,0) - v_3(x), \qquad 0 < x < \infty \tag{59}$$

$$w_3(0,y) = 0, \qquad 0 < y < \infty \tag{60}$$

$$\lim_{x \to \infty} w_3(x,y) = 0, \qquad 0 < y < \infty \tag{61}$$

The solution to (58)-(61) is given by

$$w_3(x,y) = \int_0^\infty [u_1(\xi,0) - v_3(\xi)] G^*(x,\xi,y) d\xi, \qquad 0 < x < \infty, \quad 0 < y < \infty \tag{62}$$

where the Green function G^* is defined

$$G^*(x,\xi,y) \doteq \frac{1}{\sqrt{4\pi y}} \left(\exp\left(\frac{-(x-\xi)^2}{4y} \right) - \exp\left(\frac{-(x+\xi)^2}{4y} \right) \right)$$

Shifting back to ρ and τ yields the result

$$w_3(\rho,\tau) = \int_{\rho_p}^\infty [u_1(\eta,\tau_p) - v_3(\eta)] \left(\frac{\exp\left[\frac{-(\rho-\eta)^2}{4(\tau-\tau_p)}\right] - \exp\left[\frac{-(\rho+\eta-2\rho_p)^2}{4(\tau-\tau_p)}\right]}{\sqrt{4\pi(\tau-\tau_p)}} \right) d\eta, \qquad \begin{matrix} \rho_p < \rho < \infty \\ \tau_p < \tau < \infty \end{matrix} \tag{63}$$

The final solution to (6)-(9) is then

$$C_3(\rho,\tau) = \frac{\rho_p C_p}{\rho} + \frac{1}{\rho} \int_{\rho_p}^\infty [\eta C_1(\eta,\tau_p) - \rho_p C_p] \left(\frac{\exp\left[\frac{-(\rho-\eta)^2}{4(\tau-\tau_p)}\right] - \exp\left[\frac{-(\rho+\eta-2\rho_p)^2}{4(\tau-\tau_p)}\right]}{\sqrt{4\pi(\tau-\tau_p)}} \right) d\eta, \qquad \begin{matrix} \rho_p < \rho < \infty \\ \tau_p < \tau < \infty \end{matrix} \tag{64}$$

The mass-transfer rate, equal to the mass flux times the surface area of the spherical shell, is given by

$$\dot{M}_i(r,t) = -4\pi r^2 \epsilon D \frac{\partial C_i(r,t)}{\partial r}, \qquad i = 1,2,3 \tag{65}$$

where i=1,2 or 3 depending on the space-time region of interest. The dimensionless mass-transfer rate is defined here to be

$$\dot{m}_i \doteq \frac{\dot{M}_i}{4\pi r_o \epsilon D C_o}, \qquad i = 1,2,3 \tag{66}$$

In dimensionless terms

$$\dot{m}_i(\rho,\tau) = -\frac{\rho^2}{C_o}\frac{\partial C_i(\rho,\tau)}{\partial \rho}, \qquad i = 1,2,3 \tag{67}$$

Substituting $C_i(\rho,\tau)$ in for the three space-time domains yields, respectively

$$\dot{m}_1(\rho,\tau) = \frac{\alpha}{\alpha'}\text{erfc}\left(\frac{\rho-1}{2\sqrt{\tau}}\right) + \left(\alpha\rho - \frac{\alpha}{\alpha'}\right)\exp\left(\frac{-(\rho-1)^2}{4\tau}\right)\text{F}\left(\frac{\rho-1}{2\sqrt{\tau}} + \alpha'\sqrt{\tau}\right), \qquad \begin{matrix} 1 < \rho < \infty \\ 0 < \tau < \tau_p \end{matrix} \tag{68}$$

where

$$\text{F}(x) \doteq \exp(x^2)\text{erfc}(x)$$

$$\dot{m}_2(\rho,\tau) = b + \sum_{n=1}^{\infty} A_n \left(\sin\left(\sqrt{\lambda_n}[\rho_p - \rho]\right) + \rho\sqrt{\lambda_n}\cos\left(\sqrt{\lambda_n}[\rho_p - \rho]\right)\right)\psi_n(\tau), \qquad \begin{matrix} 1 < \rho < \rho_p \\ \tau_p < \tau < \infty \end{matrix} \tag{69}$$

$$\dot{m}_3(\rho,\tau) = \rho_p \frac{C_p}{C_o} + \int_{\rho_p}^{\infty} \frac{1}{C_o}[\eta C_1(\eta,\tau_p) - \rho_p C_r]$$

$$\times \left(\frac{\left(1 + \frac{\rho(\rho-\eta)}{2(\tau-\tau_p)}\right)\exp\left(\frac{-(\rho-\eta)^2}{4(\tau-\tau_p)}\right) - \left(1 + \frac{\rho(\rho+\eta-2\rho_p)}{2(\tau-\tau_p)}\right)\exp\left(\frac{-(\rho+\eta-2\rho_p)^2}{4(\tau-\tau_p)}\right)}{\sqrt{4\pi(\tau-\tau_p)}}\right) d\eta, \qquad \begin{matrix} \rho_p < \rho < \infty \\ \tau_p < \tau < \infty \end{matrix} \tag{70}$$

4. Numerical Illustrations

Figure 3 shows the effect of a stationary precipitation front on the time-dependent dissolution rate and release rate of the solubility-limited contaminant (UO_2 in the case of spent nuclear fuel). The normalized mass-transfer rate at the waste surface (upper curves), and the normalized mass-transfer rate outward from the precipitation front (lower curves) are plotted against dimensionless time with the location of the precipitaion front as a parameter. The start of precipitation, τ_p, is indicated by the vertical bars.

The mass-transfer rates $\dot{M}$ [M/t] are normalized by the constant $4\pi\epsilon r_o D C_o$ [M/t]. Dimensionless time τ is obtained by dividing actual time by $K r_o^2/D$ [t]. For the sample values $K = 1000$, $r_o = 0.5$ m, $D = 10^{-5}\text{cm}^2/\text{s}$,

the time constant is about 8000 years. This means that the actual time scale on the figures would extend from about 10^{-2} to 10^{6} years. The mass-transfer normalization constant corresponds to the steady-state release rate from a waste sphere if no precipitation occurs away from the waste surface.

For this figure, the modified reaction-rate modulus $\alpha = j_o r_o / \epsilon D C_o$ has been set at 5000. If the precipitation front is close to the waste surface, precipitation starts soon and steady state is reached early. The mass-transfer rate at the waste surface at steady state is about 100 times higher for the precipitation front at $(r_p - r_o)/r_o = 0.01$ than for the precipitation front at $(r_p - r_o)/r_o = 10$ or for no precipitation front. If there is no precipitation front, the normalized steady-state rate at the waste surface is unity. The precipitation front acts as a sink for dissolved contaminants. When it is located nearer the waste it increases the concentration gradient and dissolution rate.

The mass-transfer rate leaving the front rises from zero at early time until the onset of precipitation at τ_p, falling thereafter to the steady state value (in real dimensions) $4\pi\epsilon r_p D C_p$. The steady-state mass release rate outside the precipitation front will be greater than that for no region of higher solubility by the ratio r_p/r_o.

The mass-transfer rate into the front is the same by definition as the rate leaving the front for $t < t_p$ when there is no precipitation occurring. After the onset of precipitation, though not shown in Figure 3, the rate into the front quickly rises to the same steady-state value as the steady-state mass-transfer rate from the waste, assuming no radioactive decay.

We see in Figure 3 that the steady-state rates leaving the front are many orders of magnitude less than the steady-state rates leaving the waste and entering the front. This indicates that nearly all the dissolved contaminant is precipitated and immobilized at the front.

As shown in Figure 4, a reduction of α to 500 reduces the early-time dissolution rate, when compared with Figure 3, due to the decrease in the rate of the forward dissolution reaction. The steady-state mass-transfer rate at the waste surface for $(r_p - r_o)/r_o = 0.01$ is also slightly lower than in Figure 3.

In Figure 5, α is reduced still further to 50, accompanied by additional lowering of the upper curves. The effect of reaction rate on the steady-state dissolution rate is more pronounced when the precipitation front is near the source. Thus, a precipitation front very near the waste surface can change what is otherwise a solubility-limited diffusion-controlled release rate to a release rate controlled by chemical reaction.

5. Conclusion

In this report we have analysed the effect of precipitation on the dissolution and transport rates of a non-decaying contaminant. Precipitation near the waste surface can have a profound effect on dissolution and transport rates. At early times, the mass-transfer rate at the waste surface is controlled by the solid-liquid reaction rate to an extent determined by the modified reaction-rate modulus, α. At later times extending to steady state, the mass-transfer rate depends on the location of the precipitation front r_p and on the solubility ratio C_o/C_p. A precipitation front very near the waste surface can change the dissolution mechanism from solubility-diffusion-controlled to chemical-reaction-rate controlled.

Precipitation limits the concentration of the contaminant at $r > r_p$ to C_p, steepening the concentration gradient for dissolution on the waste package side of the front and flattening the gradient for transport in the region outside the front. This increases the rate of contaminant transport from the waste to the front while decreasing the rate of transport away from the front, when compared to the situation without precipitation. The difference in the transport rates at the front is the rate of precipitation. For large changes in solubility, most of the contaminant is immobilized by precipitation, as was observed in a parallel study.[8]

The effect of a precipitation front located nearby in surrounding rock is to increase the release rate at the waste surface/rock interface. The increase in release rate at the waste surface is greater the closer the precipitation and the larger the ratio C_o/C_p, also observed by others.[2,3,4,5,6] The release rates of other waste constituents that dissolve congruently with the solubility-controlling matrix can be increased by a local high-solubility region between the waste surface and the precipitation front. This study has identified the main parameters of precipitation that can affect release rates.

Although the analysis has been formulated here for a sharp precipitation front, the results can be applicable if the solubility decreases with distance from the waste surface in some known fashion. As such this type of analysis may be applicable to the potential high-level nuclear waste repository. Precipitation may occur as contaminants leave hotter regions near the waste into cooler regions and it may occur if moisture penetrates the waste container, where there can be large spatial variations in oxidation potential.

References

1. U. S. NUCLEAR REGULATORY COMMISSION, Disposal of High-Level Radioactive Wastes in Geologic Repositories, 10 *Code of Federal Regulations* 60.113(a)(1)(ii)(B).
2. N. C. GARISTO & F. GARISTO, "The Effect of Precipitation on the Long-Term Release of Radionuclides from Used Fuel," *Ann. Nuc. Energy, 13*, 591, (1986).

3. F. GARISTO, "Solid Dissolution: Effect of Mass Transport-Precipitation Coupling," *Chem. Eng. Sci., 41*, 3219, (1986).

4. F. GARISTO & N. C. GARISTO, "The Effect of Precipitation on Radionuclide Release from Used Fuel," *Proc. 2nd Intl Conf. on Radioactive Waste Management*, 645, (1986).

5. N. C. GARISTO, K. B. HARVEY, F. GARISTO & L. H. JOHNSON, "Source Term Models for the Assessment of Nuclear Fuel Waste Disposal in Canada," in *Waste Mgt. '86, 2*, 397, (1986).

6. N. C. GARISTO & F. GARISTO, "Mass Transport-Precipitation Coupling in Finite Systems," AECL-9562 (1988).

7. I. NERETNIEKS, "The Movement of a Redox Front Downstream From A Repository For Nuclear Waste", *Nuclear Technology, 62*, 110, (1983).

8. I. NERETNIEKS & B. ÅSLUND, "The Movement of Radionuclides Past a Redox Front", KBS TR 83-66, (1986).

9. P. L. CHAMBRÉ, Unpublished (1987).

10. M. ABRAMOWITZ & I. A. STEGUN (eds.), *Handbook of Mathematical Functions*. New York, Dover, (1965).

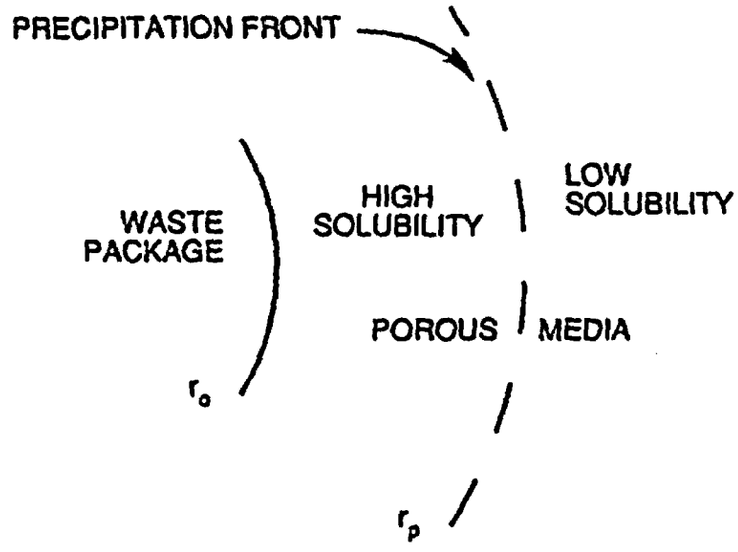

Figure 1. The stationary precipitation front.

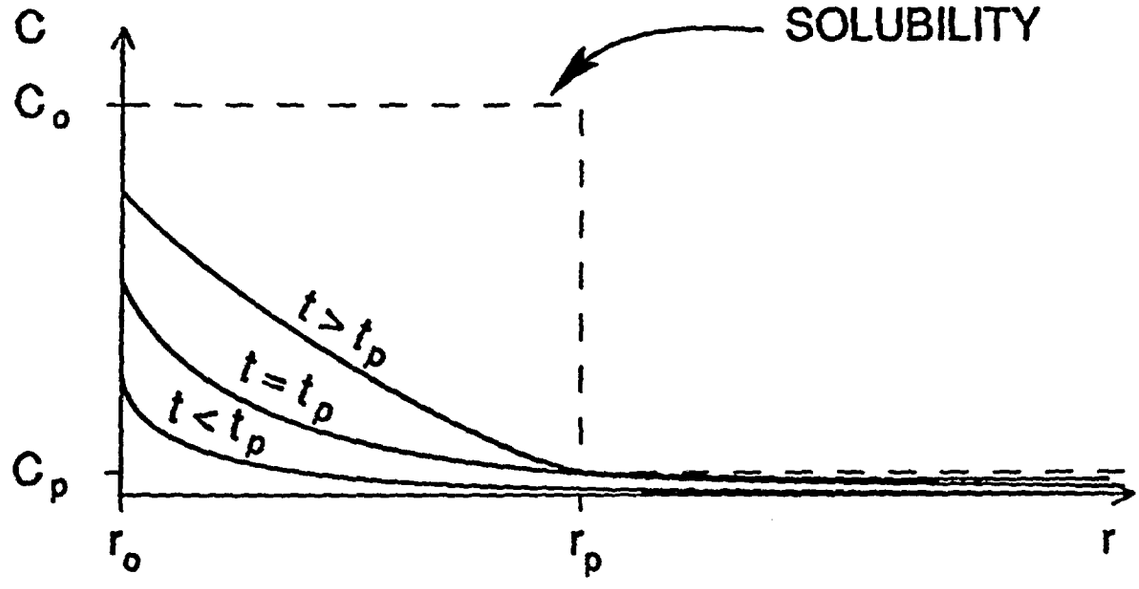

Figure 2. Schematic of concentration profiles.

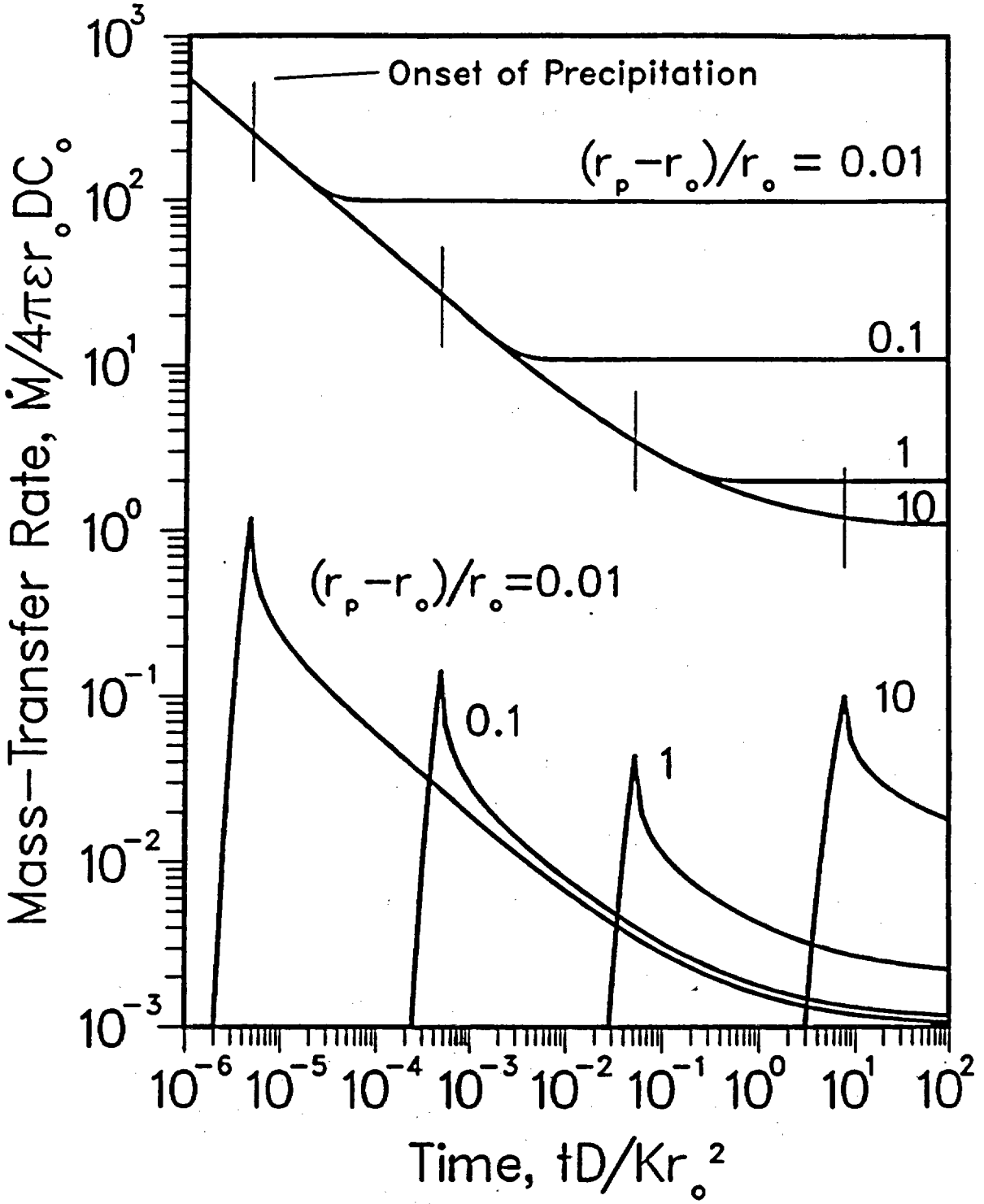

Figure 3. Dimensionless mass–transfer rate out from waste surface (upper curves) and precipitation front (lower curves) for α=5000, C_o/C_p=1000.

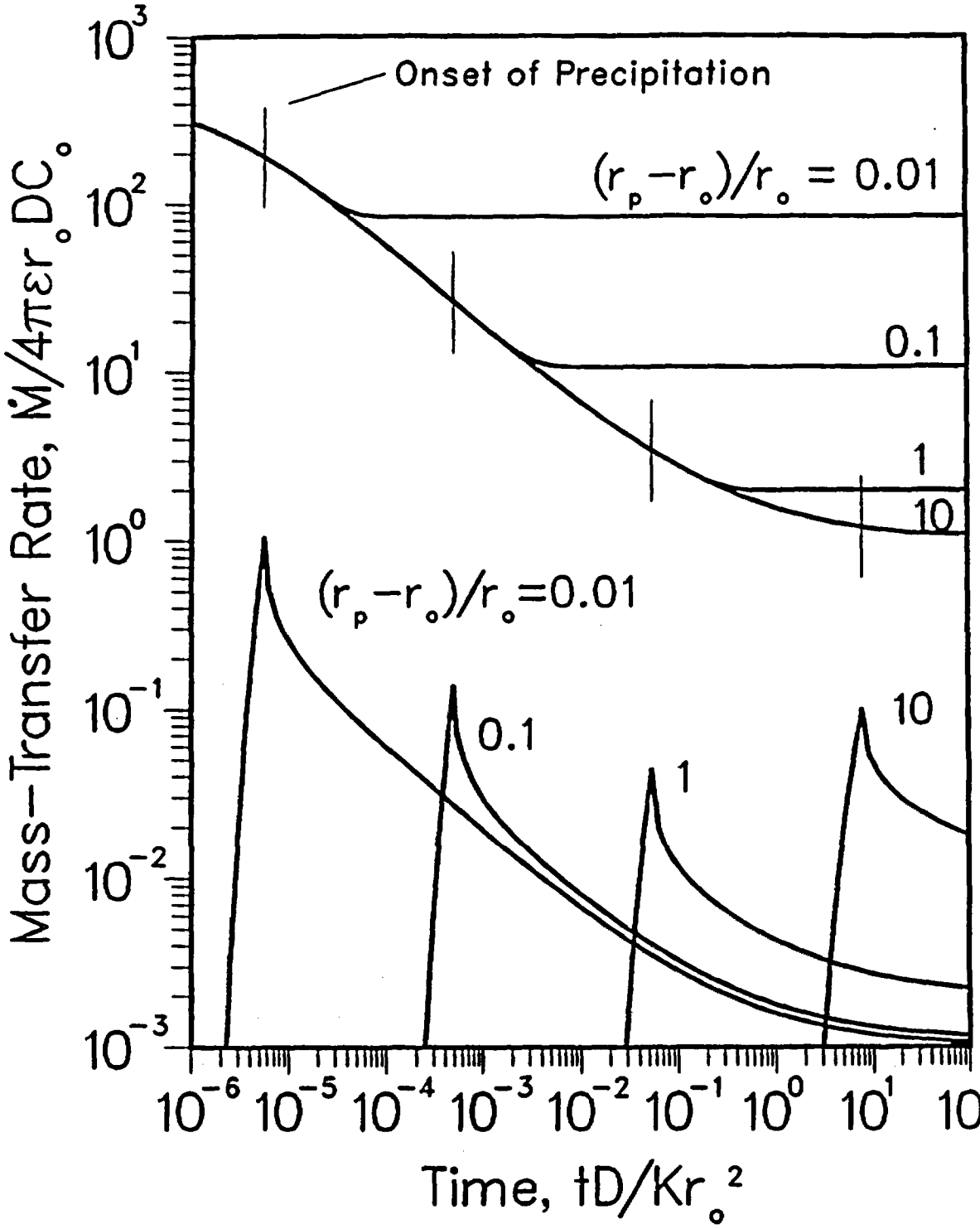

Figure 4. Dimensionless mass-transfer rate out from waste surface (upper curves) and precipitation front (lower curves) for α=500, C_o/C_p=1000.

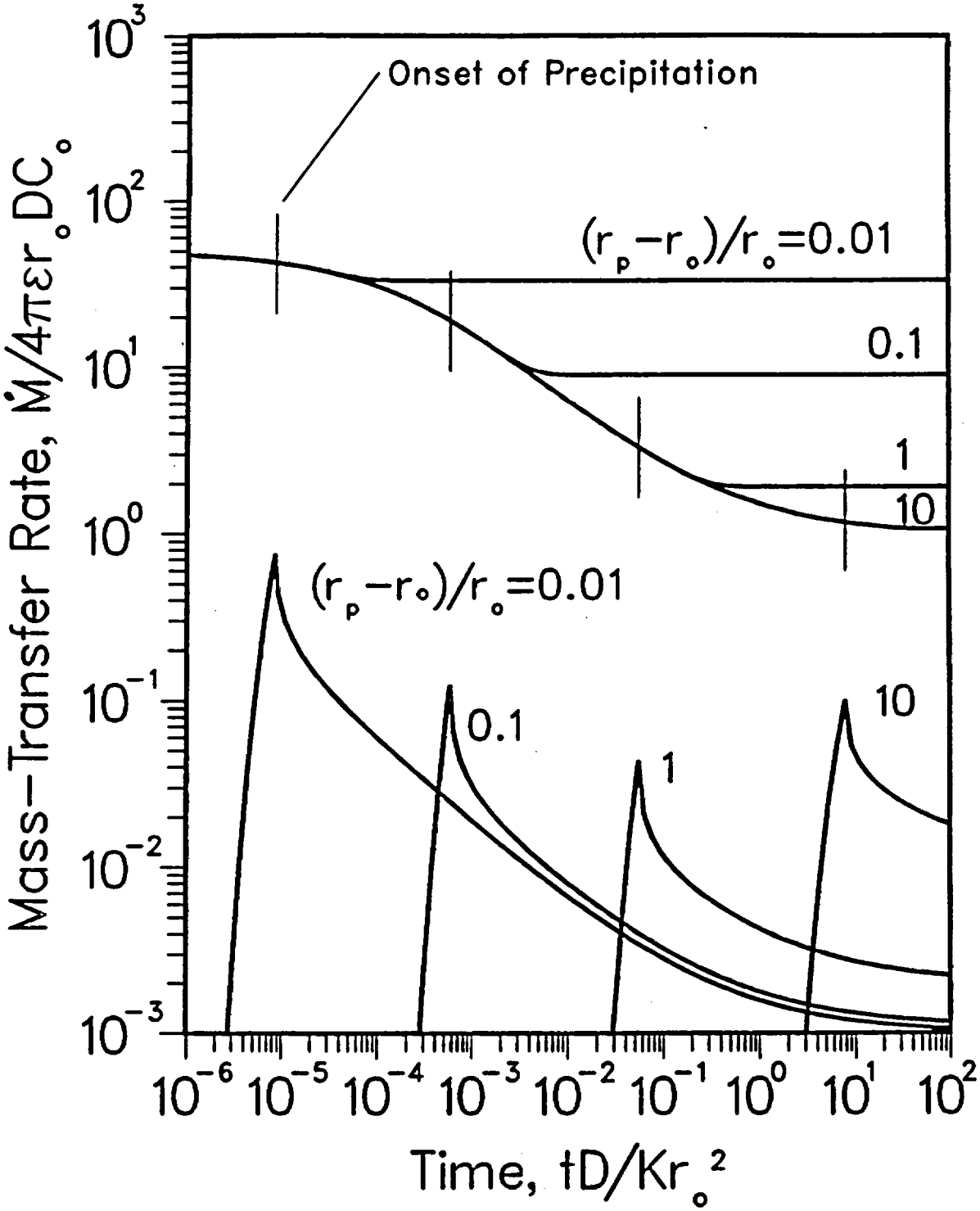

Figure 5. Dimensionless mass-transfer rate out from waste surface (upper curves) and precipitation front (lower curves) for α=50, C_o/C_p=1000.

LAWRENCE BERKELEY LABORATORY
TECHNICAL INFORMATION DEPARTMENT
UNIVERSITY OF CALIFORNIA
BERKELEY, CALIFORNIA 94720